

## Research Paper

## Time-dependent load transfer behavior of grouted anchors in laterite

Changfu Chen<sup>a,b</sup>, Shimin Zhu<sup>a,b,\*</sup>, Genbao Zhang<sup>c</sup>, Fengshan Mao<sup>a,b</sup>, Huan Cai<sup>a,b</sup><sup>a</sup> Key Laboratory of Building Safety and Energy Efficiency of the Ministry of Education, Hunan University, Changsha 410082, PR China<sup>b</sup> College of Civil Engineering, Hunan University, Changsha, Hunan 410082, PR China<sup>c</sup> College of Civil Engineering, Hunan City University, Yiyang, Hunan 413000, PR China

## ARTICLE INFO

## Keywords:

Laterite  
Grouted anchors  
Time effect  
Merchant model  
Load transfer behavior

## ABSTRACT

The load transfer behavior of grouted anchors is time-dependent under long-term (creep) load. This study aims at investigating the time-dependent behavior of grouted anchors in laterite by both physical model test and theoretical simulation. A laboratory creep pullout model test of full-length-bond grouted anchor in laterite was carried out using a special developed apparatus. The creep pullout load–displacement response at anchor head and time history curves of axial strain were tested and presented. The creep behavior on the grout - soil interface was simulated using Merchant rheological model in theoretical simulation. By comparing the experimental data with predictions, the applicability of the proposed theoretical method was validated, and the time-dependent load transfer behavior of grouted anchors was discussed. The impacts of five model parameters on the time-dependent pullout response were further analyzed by parametric studies. It revealed that the tensile force distribution tends to be linear, and the shear stress distribution towards uniformity as time elapsed. Additionally, the time-dependent load transfer behavior for grouted anchors is influenced by the above parameters in various levels. This work provides insights into understandings of time-dependent behavior, and facilitates the service life design practice for grouted anchors embedded in laterite.

## 1. Introduction

Laterite refers to a type of maroon clay formed by the weathering (or laterization) of carbonate rocks or rocks rich in iron and aluminum oxides in hot and humid climates (Tan and Kong, 2006; Lin, 1989), which exists widely in humid areas with abundant rainfall in Southern China (Huang and Fu, 1998; Cheng et al., 2004). In recent decades, a large number of laterite slopes supported by grouted anchors have been formed in Southern China owing to the plentiful construction of basic infrastructural facilities, such as tunnels, railways, etc. (Zhang et al., 2015, 2018; Chen et al., 2014; Luo et al., 2003; Ehrlich and Silva, 2015). Laterite has the characteristics of easy softening in water, strong plasticity and easy creep because of a high content of hydrophilic minerals (Zhang et al., 2015; Chen et al., 2014, 2019; Zhu et al., 2019). Consequently, the time-dependent mechanical behaviors (creep and stress relaxation) of grouted anchors become the key factor in determining the long-term stability of anchored laterite slopes.

The mechanical properties of grouted anchors are decisively dependent on the grout - soil interface shear behavior. Previous studies

on interface shear behavior (Hong et al., 2017; Borana et al., 2017; Kim et al., 2013; Zhu et al., 2011; Chu and Yin, 2005; Su et al., 2010; Chen et al., 2015; Gurpersaud et al., 2013; Ye et al., 2017) or load transfer behavior of grouted anchors (Farmer, 1975; Hong et al., 2017; Huang et al., 2012; Ren et al., 2010; Martín et al., 2011; Ma et al., 2016; Chen et al., 2019) mainly focused on the working condition with short-term load. However, when adopting grouted anchors as long-term supporting structures in geotechnical engineering, much attention shall be paid on the time-dependent behavior (including creep (Chen et al., 2016; Zhang et al., 2015) or stress relaxation (Shi et al., 2019; Chen et al., 2018)). Otherwise, rheological damage could occur during the service period (Yang et al., 2014).

The creep phenomena of grouted anchors comes down to tensile creep of the anchor bar, shear creep of the surrounding soil and shear creep on the grout - soil interface. Among them, the interface shear behavior between grout and soil is the most intricate point that directly determines the long-term bearing capacity of grouted anchors (Chen et al., 2016). Some researchers have studied the influence of various factors (such as physical properties of soil (Zhang et al., 2020); grouting

\* Corresponding author at: College of Civil Engineering, Hunan University, Changsha, Hunan 410082, PR China.

E-mail addresses: [cfchen@hnu.edu.cn](mailto:cfchen@hnu.edu.cn) (C. Chen), [smzhu@hnu.edu.cn](mailto:smzhu@hnu.edu.cn) (S. Zhu), [gbzhang@hnu.edu.cn](mailto:gbzhang@hnu.edu.cn) (G. Zhang), [mfangshan@hnu.edu.cn](mailto:mfangshan@hnu.edu.cn) (F. Mao), [caihuan@hnu.edu.cn](mailto:caihuan@hnu.edu.cn) (H. Cai).

<https://doi.org/10.1016/j.compgeo.2020.103969>

Received 14 June 2020; Received in revised form 19 October 2020; Accepted 5 December 2020

Available online 16 January 2021

0266-352X/© 2021 Elsevier Ltd. All rights reserved.

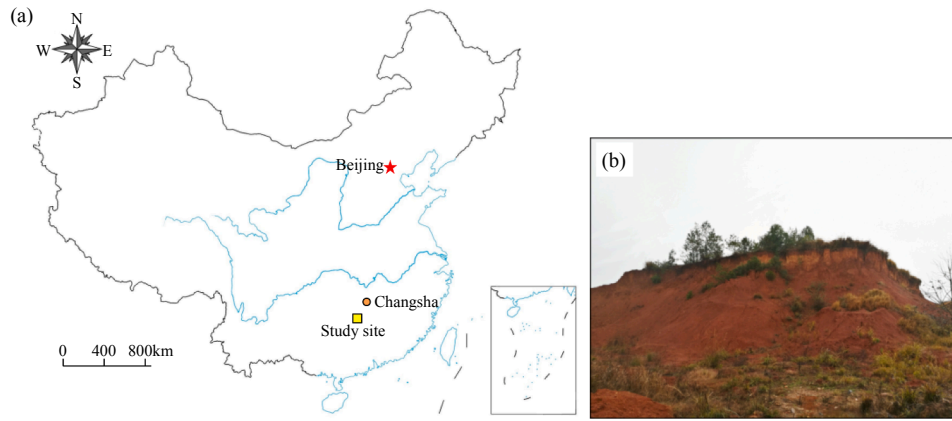


Fig. 1. The soil collection site: (a) location illustration; (b) a view of the stratum in study site.

pressure (Chen et al., 2019) and in-service environment (EI Menoufy and Soudki, 2014) on the interface shear creep behavior between grout and soil through long-term (creep) pullout tests for element specimens of grouted anchors. Furthermore, for characterizing the interface creep behavior of the grouted anchors, several rheological models (such as empirical rheological model with hyperbolic form (Chen et al., 2016), hybrid rheological model (Zhang et al., 2020); kriging method-based creep model (Chen et al., 2019) and damage creep model (Xu et al., 2002); modified Burgers model (Kränkel et al., 2015) were typically established based on corresponding testing results.

In general, the stress distributions of grouted anchors are nonlinear (Farmer, 1975). The existing theoretical studies on time-dependent load transfer behavior of grouted anchors generally assumed that the geotechnical materials or structural materials are rheological, such as tensioned bars (Zhang et al., 2015); grouting material (Yang et al., 2014) and soil (Wu, 2009). Based on these assumptions, time-dependent distributions of both tensile force and shear stress could be deduced via load transfer method. However, for grouted anchors embedded in laterite, the creep destruction was mostly occurred in the interface region, and creep deformation of the anchor is relatively small and controllable compared with the interface shear creep displacement between grout and soil. Therefore, it would be more appropriate to consider the interface shear creep behavior between grout and soil in the simulation, whereas relevant studies are not yet reported.

In order to study the time-dependent load transfer behavior of grouted anchors in laterite, a special creep pullout test apparatus was developed in present work. A creep pullout model test of full-length-bond grouted anchors was carried out using this apparatus. The creep pullout load–displacement response at anchor head and time history curves of axial strain were obtained. Red clay (one type of laterite) collected from Hengyang red beds basin, Hunan Province, China, was used in this study, whose chemical composition, mineral composition and basic mechanical properties were tested. The Merchant rheological model was utilized as constitutive model for simulating the creep interaction between grout and soil. By comparing the experimental data with the predictions, the proposed theoretical analysis method turned to be effective and practical. Additionally, the effects of bond length, axial stiffness and three rheological model parameters on the time-dependent mechanical behavior of grouted anchors were further studied parametrically.

## 2. Long-term (creep) pullout model test of grouted anchors in laterite

### 2.1. Material properties

The soil used in this test was taken from a weathered eluvium located

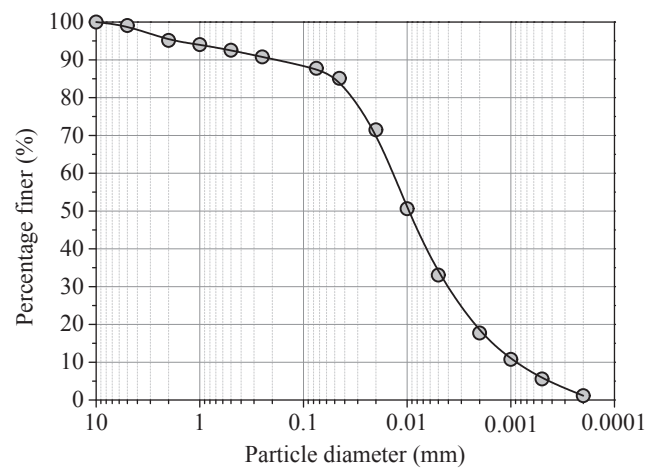


Fig. 2. Particle-size distribution curve of the collected laterite.

Table 1

Material properties of the collected laterite, reinforcement bar and cement grouted material.

Soil sample	Units	Values
Natural water content ( $w$ )	%	30.6
Natural density ( $\rho$ )	Mg/m <sup>3</sup>	16.4
Natural dry density ( $\rho_d$ )	g/cm <sup>3</sup>	1.20
Natural void ratio ( $e$ )		1.21
Specific gravity ( $G_s$ )		2.693
Liquid limit ( $w_l$ )	%	57.3
Plasticity limit ( $w_p$ )	%	33.9
Plasticity index ( $I_p$ )	%	23.4
Maximum dry density ( $\rho_{dmax}$ )	g/cm <sup>3</sup>	1.53
Optimum water content ( $w_{opt}$ )	%	25.1
Cohesion ( $c$ )	kPa	49.1
Internal friction angle ( $\phi$ )	°	16.7
Modulus of compression ( $E_c$ )	MPa	2.77
<b>Reinforcement bar</b>		
Type		Hot-rolled ribbed bar
Nominal diameter ( $d_n$ )	mm	18
Elasticity modulus ( $E$ )	GPa	210
<b>Grout</b>		
Cement type		P.O 42.5
Water cement ratio ( $\alpha$ )		1:0.45
Compressive strength ( $q_u$ )	MPa	30.5
Elasticity modulus ( $E_c$ )	GPa	13.5

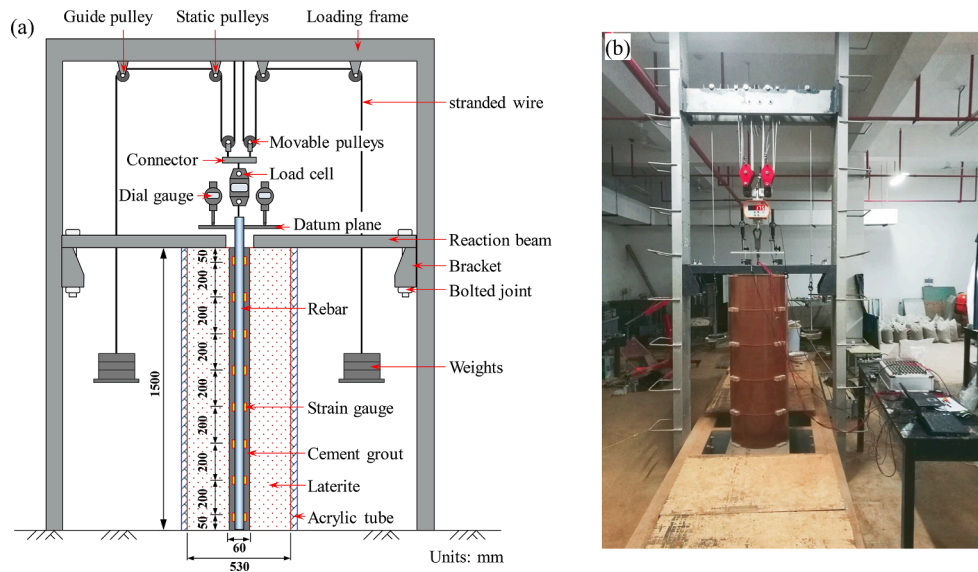


Fig. 3. Views of creep pullout test setup: (a) schematic illustration; (b) photograph.

in the Hengyang red beds basin of Hunan province, China (Fig. 1), which appears to be maroon. Chemical composition of the collected soil was obtained by X-Ray Fluorescence Spectrometer (XRF), which was: silica ( $\text{SiO}_2$ ) (46.5%), alumina ( $\text{Al}_2\text{O}_3$ ) (25.5%), ferric oxide ( $\text{Fe}_2\text{O}_3$ ) (13.3%), potassium oxide ( $\text{K}_2\text{O}$ ) (2.3%), titanium dioxide ( $\text{TiO}_2$ ) (1.4%), magnesium oxide ( $\text{MgO}$ ) (0.6%) and ignition loss (10.4%). Mineral composition of the collected soil was obtained by X-Ray Diffraction (XRD), which was: quartz (39.5%), kaolinite (28.8%), hematite (17.4%), mica (8.4%), anatase (3.2%) and rutile (2.8%). This soil samples can be identified as laterite from the chemical composition and mineral composition in soil classification (Tan and Kong, 2006; Lin, 1989). The particle-size distribution and basic properties of the soil were tested and specifically presented in Fig. 2 and Table 1. The natural void ratio  $e$  of the soil is 1.21 (greater than 1.0), and the plasticity index  $I_p$  is 23.4 (greater than 20). Therefore, the soil can be further determined to be red clay (one type of laterite) from natural void ratio  $e$  and plasticity index  $I_p$  (Tan and Kong, 2006; Lin, 1989). According to the one-dimensional consolidation test results of undisturbed soil samples, the studied soil is highly compressible with a compression modulus  $E_s$  of 2.77 MPa.

Generally, physical model tests need large quantity of soil, which brings great challenges to the exploration, collection and transportation of uniform undisturbed soil. In addition, soils would be inevitably disturbed and its structure would also be damaged during the construction process, including creating hole and grouting. Hence, the laterite samples prepared at remolded state with moisture content of 30% was used throughout the testing program. Specifically, the collected laterite was cleaned from foreign materials, and only particles passing through the 5-mm sieve were preserved. It is worth noted that testing results and conclusions based on remolded soil in this work can be adequately referred for cases with undisturbed soil in practice, in particular due to the low structure-sensibility of laterite.

The reinforcement bar was hot-rolled ribbed bar with nominal diameter of 18 mm, and a circular steel hook was welded at the end of the bar for facilitating loading. The grouted material was cement paste with water cement ratio  $\alpha$  of 0.45. It should be noted that polycarboxylic super-plasticizer (0.25%) was also added to the grouted material to increase its liquidity and make it easy for grouting. Properties of the reinforcement bar and grouted material are also given in Table 1.

## 2.2. Test setup

Creep pullout test setup is composed of pulley system and data acquisition system, as shown in Fig. 3. The pulley system was designed from inspiration of assembly pulley, mainly consisting of a loading frame, a series of pulleys and steel wire. Two groups of static pulleys and movable pulleys were assembled on both sides of the model specimen symmetrically, which can amplify the applied long-term (creep) load provided by weights up to 10 times. The data acquisition system included two displacement gauges, a DH3816 strain measuring device and a load cell. The two displacement gauges were symmetrically placed on both sides of the exposed section of reinforcement bar to monitor the creep pullout displacement of the anchor head. There were eight pairs of strain gauges attached on the bonding section of reinforcement bar with the interval of 0.2 m to monitor the distribution of axial strain.

Before conducting the physical model tests, a cylindrical soil column with a length of 1500 mm, an outer diameter of 530 mm and an anchor hole diameter of 60 mm was prepared in an acrylic tube in advance. The acrylic tube was cut into five short sections and can be connected tightly with nuts as a whole. Generally, the influence zone of lateral friction resistance of a pile is between 5 and 10 times of pile diameter (Cooke et al., 1979), and grouted anchors are similar to piles in shapes and mechanisms. In this physical model test, the ratio of the outer diameter of specimen (530 mm) to the diameter of anchor hole (60 mm) was 8.8. Hence, the impact of boundary effect could be almost eliminated, and the boundary conditions in physical model and the following numerical model are basically consistent. Besides, a reaction beam was installed on the top of the model specimen to avoid unnecessary swing and facilitate loading.

## 2.3. Testing procedures

The existing testing method of long-term (creep) pullout test for element grouted anchors (Chen et al., 2016, 2019; Zhang et al., 2020) was imitated and improved in this work. The main steps of testing procedures include plastering strain gauges; specimen molds assembly, soil compaction in layers, anchor hole creating, grouting, and long-term (creep) load application, which are presented in detail as follows.

### (a) Plastering strain gauges

Eight sets of strain gauges were plastered on the strain monitoring

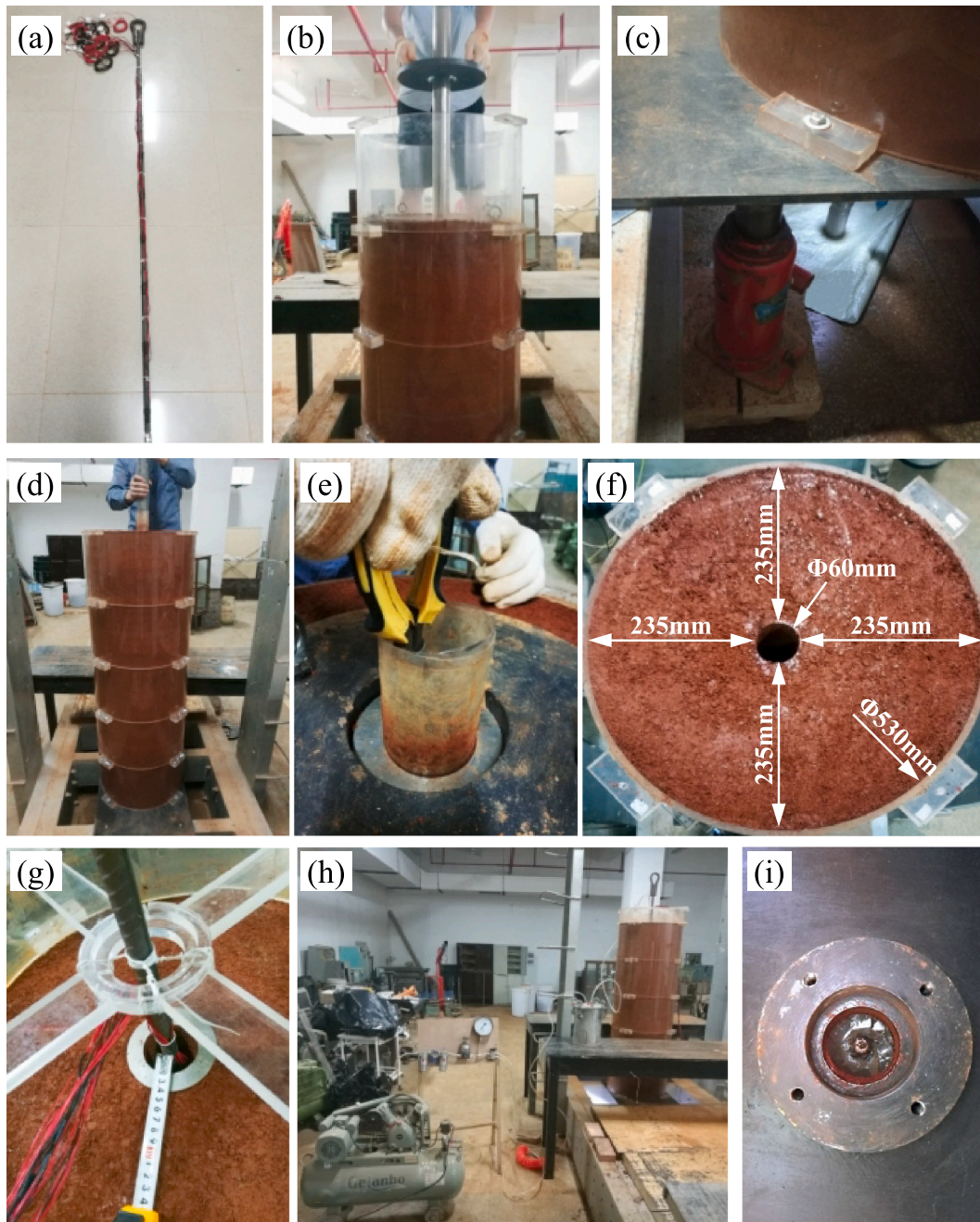


**Fig. 4.** Procedures of preparing pullout model specimen: (a) the reinforcement bar plastered with strain gauges; (b) soil compaction in layer; (c) adjusting the verticality of the steel tube; (d) pulling out the steel tube from soil specimen; (e) plastic film separating; (f) shape of the created anchor hole; (g) reinforcement bar centering; (h) grouting; (i) bottom of the specimen after grouting.

points of the reinforcement bar with quick-drying gelatin (Fig. 4(a)). After the quick-drying gelatin had been completely hardened, encapsulating these strain gauges with silica gel.

#### (b) Specimen molds assembly

A steel tube covered with plastic film that used to create the anchor hole was pre-embedded in the assembled molds. It should be noted that carbon powder was applied to the interface between the steel tube and plastic film for lubricating. The first acrylic tube and the steel tube covered with plastic film were screwed up on the chassis of the loading frame in the following.

#### (c) Soil compaction in layers

The remolded laterite with 30% water content was filled into the first acrylic tube, and was compacted in layers (Fig. 4(b)). The dry density of the laterite is  $1.20 \text{ g/cm}^3$  and the compaction thickness of each layer was controlled at 4 cm. After filling soil with the first acrylic tube, the second acrylic tube was installed on the top of the first acrylic tube with screws. The remolded laterite was filled and compacted sequentially. Repeating this process until the five acrylic tubes were all be filled. It should be noted that dry density and water content of the compacted remolded soil were almost the same as the site undisturbed soil.

#### (d) Anchor hole creating

After soil compaction, the steel tube covered with plastic film would remain in the center of the compacted soil. Using both jack and plumb

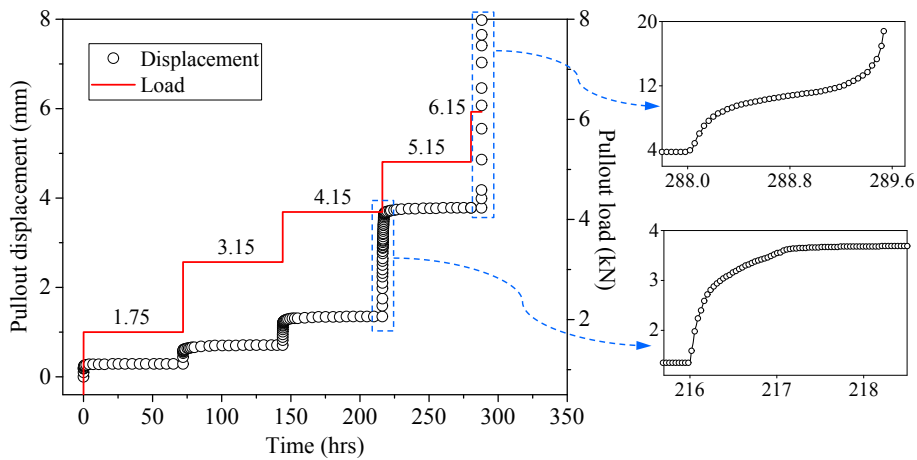


Fig. 5. Time history curve of pullout displacement of anchor head under multi-stage pullout loading.

bob to check and adjust the verticality of the steel tube (Fig. 4(c)), the anchor can be secured to be vertically positioned in the following test by aligning the gravitational verticality with the inner wall of the steel tube. Then, pulling out the steel tube from the soil specimen slowly (Fig. 4(d)), and rotating the plastic film towards the center carefully until it was completely separated from the soil (Fig. 4(e)). A uniform cylindrical hole that simulates the anchor hole was formed at the center of the soil specimen in this way (Fig. 4(f)). It should be mentioned that test result deviation caused by this precast anchor hole and drilling hole commonly used in practice was minor due to the consistent development of shear band over soil-anchor interface. In addition, the use of precast hole can ensure the verticality of hole and soil uniformity, and mitigate the test error caused by operation more effectively. Hence, this construction method has been adopted in this test and some of other pullout tests for anchors/soil nails, such as Chu and Yin (2005) and Hong et al. (2017).

(e) Grouting

A specially designed steel plug equipped with a seal ring was installed into the bottom of anchor hole for preventing the leakage of cement paste during grouting. The reinforcement bar plastered with strain gauges was placed on the center of the anchor hole, where cement paste powered by an air compressor was injected in (Fig. 4(g), (h), and (i)). It should be noted that no grouting pressure was applied in this process.

After curing for 28 days in sealed condition, the pulley system and

data acquisition system were assembled on the model specimen and loading frame, as shown in Fig. 3. A multi-stage loading method was adopted in accordance with Tan’s method (Tan and Kang, 1980). Creep curves of  $n$  loading steps were obtained from only one specimen in this loading method, which is equivalent to  $n$  one-step loadings of various load levels on  $n$  different specimens. Long-term (Creep) loads for this testing anchor were selected mainly according to the short-term (instantaneous) ultimate pullout capacity at the same conditions. Specifically, interface shear strength was measured to be 32.4 kPa from short-term (rapid) pullout tests for element-grouted anchor specimen, and the short-term ultimate pullout capacity was calculated to be 9.16 kN. Long-term loads were specified as eight levels, which are 1.75 kN, 3.15 kN, 4.15 kN, 5.15 kN, 6.15 kN, 7.15 kN, 8.15 kN, and 9.15 kN in sequence. However, the grouted anchor was completely pulled out under the load of 6.15 kN owing to the creep effect, which meant the model test was finished. It is of great significance to select an appropriate creep time scale or stability criterion in creep tests. In this paper, the next level of long-term load would be added when the displacement rate of anchor head dropped below 0.01 mm over 24 h at a given loading level, which in reference to the criterion proposed by Sun (1999). In addition, considering the long-term performance of the instruments, loading time of each level was all set as 72 h in this creep physical model test.

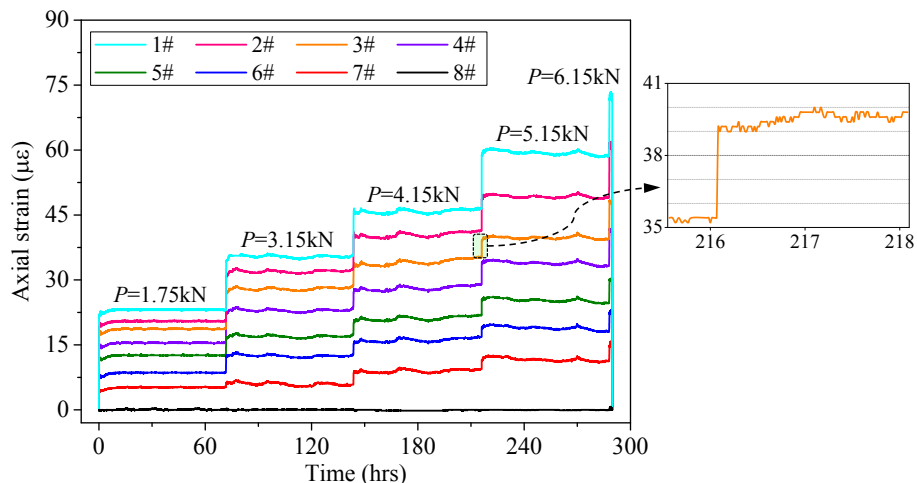


Fig. 6. Time history curves of axial strain at various positions of reinforcement bar.

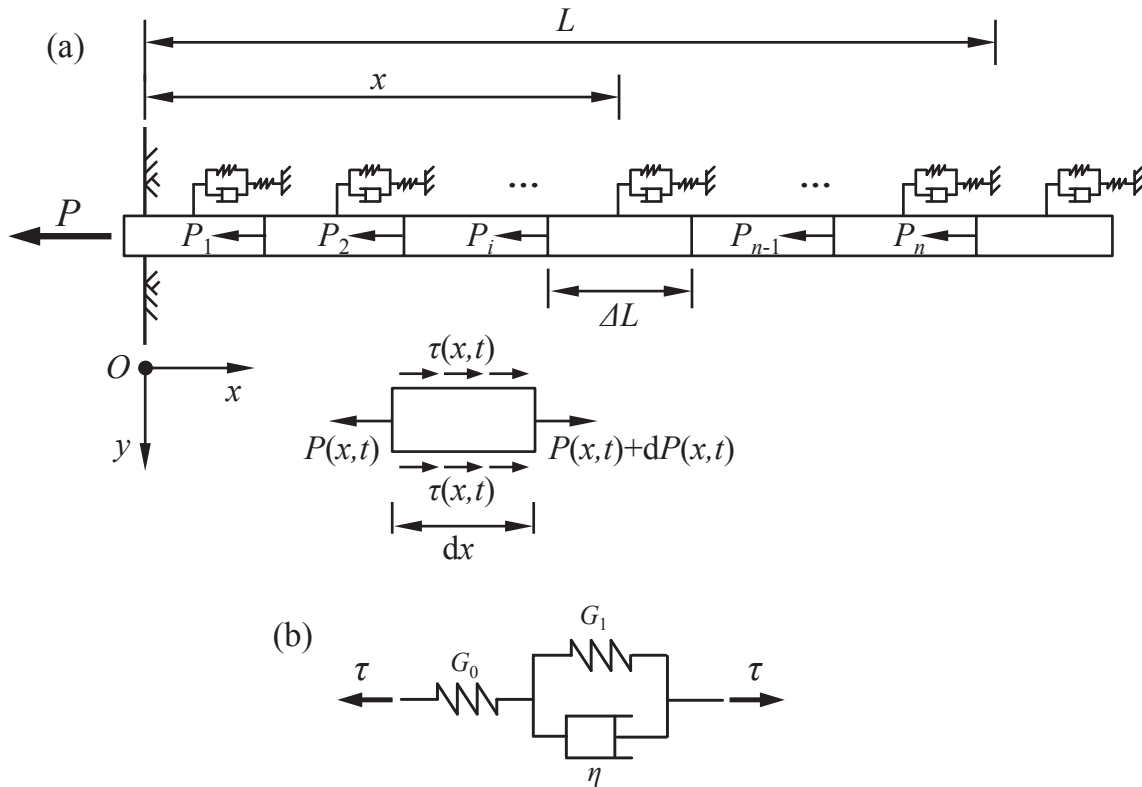


Fig. 7. Analytical schematic of time-dependent load transfer behavior for grouted anchors in laterite: (a) force analysis schematic; (b) Merchant rheological model.

2.4. Test results

Fig. 5 shows the time history curve of pullout displacement of anchor head under multi-stage pullout loads. The time history curve under multi-stage loads was transformed into a cluster of creep curves corresponding to all loading levels based on a nonlinear superposition method (Tan and Kang, 1980), as shown in Fig. 8. When the pullout load is lower than 5.15 kN, the pullout displacement develops with varying creep rate. The creep rate varies in two stages: the attenuated creep stage with decreasing creep rate and the steady creep stage with constant creep rate. The majority of the creep displacement occurs in the attenuated creep stage. Specifically, the durations of attenuated creep stage measured in the presented test are 0.1 h, 0.2 h, 0.4 h and 1.5 h for creep curves under the load of 1.75 kN, 3.15 kN, 4.15 kN and 5.15 kN, respectively. Because the duration of attenuated creep stage is much less than that of the steady creep stage, it is difficult to distinguish the creep behavior with the instant behavior in the full-range view of time history of creep displacement (i.e. creep curve). It is noteworthy that the tested anchor was pulled out with the occurrence of the accelerated creep stage (i.e. increasing creep rate) when the applied load reached 6.15 kN in the test. Continuous shear failure occurred along the grout - soil interface, which indicated the pullout displacements were almost interface shear displacements between grout and soil. Additionally, the grout surface was covered with a thin layer of surrounding laterite with an approximate thickness of 5 mm, which indicates the shear band would be developed continuously during the process of creep pullout.

Fig. 6 illustrates time history curves of axial strain of the grouted anchor at eight monitoring points. Similar to the time history curves of pullout displacement, the axial strains of all monitoring points increased rapidly and tended to be stable at last when the pullout loads is lower than 5.15 kN. It is worth noted that the monitored axial strains fluctuated within a narrow range owing to the strain measuring instrumental errors and environmental noise. When the pullout load reached 6.15 kN, the axial strains increased firstly and decreased to zero sharply after a

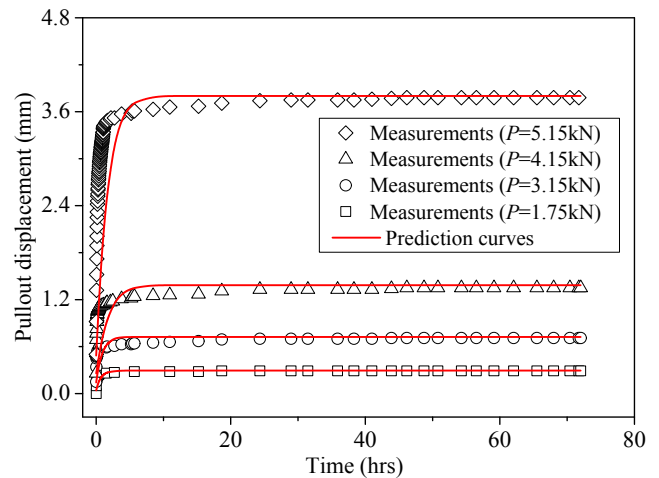


Fig. 8. Prediction for the testing pullout creep curves of anchor head.

short period of stabilization for about 2 h because of the completion of the test.

3. Time-dependent load transfer modelling of grouted anchors

The creep problem could occur in both the anchor and the grout-soil interface under long-term load. For grouted anchors in laterite, it was observed in the above physical model test results that the interface shear creep displacement is dominant compared with the tensile creep deformation of the anchor. For instance, under the load of 5.15 kN, the grout-soil interface displacement reached 3.74 mm, while the tensile deformation of the anchor was only about 0.03 mm. The reason for this phenomenon is that the axial stiffness of the anchor is much greater compared with the interface shear stiffness between the grout and soil.

Consequently, the Merchant rheological model was adopted as load transfer model to simulate the anchor creep behavior tested in this work. Additionally, the tensile deformation of the anchor is assumed to be instantaneous and elastic for its little value, which could facilitate the theoretical analysis. The time-dependent load transfer behavior of grouted anchors in laterite under low pullout load was analyzed in detail as follows.

### 3.1. Governing equation

The analytical schematic of time-dependent load transfer behavior for grouted anchors in laterite is shown in Fig. 7, from where geometric equation, physical equation, and force equilibrium equation can be reasoned.

The axial strain of the grouted anchors  $\epsilon(x,t)$  can be expressed by Eq. (1), which is the geometric equation:

$$\epsilon(x,t) = -\frac{\partial s(x,t)}{\partial x} \quad (1)$$

where  $s(x,t)$  is the axial displacement of the anchor;  $x$  is the distance from the anchor head;  $t$  is time.

The axial strain of the grouted anchors  $\epsilon(x,t)$  can also be expressed by Eq. (2), which is the physical equation. It should be noted that the tensile deformation of the anchor is assumed to be instantaneous and elastic in this work.

$$\epsilon(x,t) = \frac{P(x,t)}{EA} \quad (2)$$

where  $P(x,t)$  is the tensile force of the anchor;  $E$  and  $A$  represent Young's modulus and the cross-sectional area of the anchor respectively.

It should be noted that  $E$  is a composite modulus of the reinforcement bar and grout material for grouted anchors, and can be calculated by Eq. (3).

$$E = \frac{E_b A_b + E_g A_g}{A_b + A_g} \quad (3)$$

where  $E_b$  and  $E_g$  represent the elasticity modulus of the reinforcement bar and grout respectively;  $A_b$  and  $A_g$  represent the cross-sectional area of the reinforcement bar and grout respectively.

For a separate segment of anchor with the length of  $dx$ , The force equilibrium equation can be expressed by:

$$dP(x,t) + u_p \tau(x,t) dx = 0 \quad (4)$$

where  $\tau(x,t)$  is the interface shear stress between grout and soil;  $\mu_p$  is the perimeter of the anchor.

Eq. (4) can be converted into the following form:

$$\frac{\partial P(x,t)}{\partial x} = -u_p \tau(x,t) \quad (5)$$

Merchant rheological model is a three-component viscoelastic model, which is composed of a spring element and Kelvin model in series, as shown in Fig. 7(b). This model is widely used to characterize both creep and stress relaxation behavior (Zhang et al., 2015) of geomaterials, in particular due to its concise formulation and engineer-friendly solving process. Hence, Merchant rheological model was used to simulate the interface shear creep behavior between grout and soil. The constitutive equation of Merchant rheological model is:

$$G_1 s(x,t) + \eta \frac{\partial s(x,t)}{\partial t} = \left( \frac{G_0 + G_1}{G_0} \right) \tau(x,t) + \frac{\eta}{G_0} \frac{\partial \tau(x,t)}{\partial t} \quad (6)$$

where  $G_0$  and  $G_1$  are interface shear modulus between grout and soil;  $\eta$  is interface shear viscosity coefficient between grout and soil.

Combining Eqs. (1), (2), (5), with (6), the governing equation of time-dependent load transfer behavior for grouted anchors can be

deduced:

$$\frac{\partial}{\partial t} \left( \frac{\partial^2 s}{\partial x^2} - \frac{\mu_p G_0}{EA} s \right) + \left( \frac{G_0 + G_1}{\eta} \right) \frac{\partial^2 s}{\partial x^2} - \frac{\mu_p G_0 G_1}{EA \eta} s = 0 \quad (7)$$

Eq. (7) is a third-order partial differential equation, which is difficult to obtain its analytical solution. But the axial displacement  $s(x,t)$  can be solved using finite-difference method combined with the boundary value conditions. Furthermore, the tensile force  $P(x,t)$  and the shear stress  $\tau(x,t)$  can be calculated by Eqs. (8) and (9), respectively.

$$P(x,t) = -EA \frac{\partial s(x,t)}{\partial x} \quad (8)$$

$$\tau(x,t) = \frac{EA}{\mu_p} \frac{\partial^2 s(x,t)}{\partial x^2} \quad (9)$$

### 3.2. Boundary value conditions

Boundary value conditions of the governing equation Eq. (7) are consisted of the boundary conditions and initial conditions. When a constant pullout load (assuming to be  $P_0$ ) is exerted on the anchor head, the tensile forces at the anchor head and anchor toe are  $P_0$  and 0 respectively, which remains constant with the time. Therefore, the boundary conditions can be expressed by:

$$\begin{cases} P(x,t)|_{x=0} = P_0 \\ P(x,t)|_{x=L} = 0 \end{cases} \quad (10)$$

At the initial moment of loading, interface shear modulus between grout and soil is  $G_0$ , and the load transfer model Eq. (6) can be rewritten as:

$$\tau(x,t_0) = G_0 s(x,t_0) \quad (11)$$

where  $t_0$  represents the initial moment of loading ( $t = 0$ ).

The governing equation Eq. (7) can then be expressed by:

$$\frac{d^2 s(x,t_0)}{dx^2} - \frac{\mu_p G_0}{EA} s(x,t_0) = 0 \quad (12)$$

Eq. (12) is a second-order homogeneous differential equation with constant coefficients, and its analytical solution can be obtained:

$$s(x,t_0) = C_1 e^{\beta x} + C_2 e^{-\beta x} \quad (13)$$

where  $\beta = \sqrt{\frac{\mu_p G_0}{EA}}$ ;  $C_1$  and  $C_2$  are all undetermined parameters.

The corresponding interface shear stress and tensile force are then calculated by substituting Eq. (13) into Eqs. (11) and (8), respectively.

$$\tau(x,t_0) = G_0 (C_1 e^{\beta x} + C_2 e^{-\beta x}) \quad (14)$$

$$P(x,t_0) = \beta EA (C_2 e^{-\beta x} - C_1 e^{\beta x}) \quad (15)$$

$C_1$  and  $C_2$  are calculated by substituting Eq. (10) into Eq. (15). Furtherly, Eqs. (13), (14) and (15) can be rewritten as Eq. (16), which corresponds to the initial conditions of the load transfer analysis. It should be noted that Eqs. (10) and (16) are the boundary value conditions for solving the governing equation Eq. (7).

$$\begin{cases} s(x,t_0) = \frac{P_0}{(e^{2\beta L} - 1)\beta EA} (e^{\beta x} + e^{2\beta L - \beta x}) \\ \tau(x,t_0) = \frac{G_0 P_0}{(e^{2\beta L} - 1)\beta EA} (e^{\beta x} + e^{2\beta L - \beta x}) \\ P(x,t_0) = \frac{P_0}{(1 - e^{2\beta L})} (e^{\beta x} - e^{2\beta L - \beta x}) \end{cases} \quad (16)$$

Additionally, when time  $t$  tends to be infinite  $t_{\infty}$ , the ultimate displacement  $s_{\infty}$  of the Merchant model can be expressed by Eq. (17).



**Table 2**  
Parameters of Merchant rheological model used for simulating model test results.

Model parameters	$P_0$ (kN)			
	1.75	3.15	4.15	5.15
$G_0$ (MPa)	200	90	63	40
$G_1$ (MPa)	26	20	13.5	5.6
$\eta$ (MPa-h)	25	20	15	10

**Table 3**  
Parameters design in parametric studies.

Parameter	$L$ (m)	$G_0$ (MPa)	$G_1$ (MPa)	$\eta$ (MPa-h)	$EA$ (MN)
$L$	1.5/3/6/ 9/12/15/ 18	40	5.6	10	88.2
$G_0$	6	40/30/ 20/10/5	5.6	10	88.2
$G_1$	6	40	1.4/2.8/ 5.6/8/12	10	88.2
$\eta$	6	40	5.6	10/30/50/ 70/90	88.2
$E$	6	40	5.6	10	88.2/56.5/ 28.3/14.2/ 7.1

curves of anchor head obtained from the above model test. The obtained model parameters are shown in Table 2. Only the attenuation creep curves are analyzed, which are corresponding to the first to fourth loading stages (1.75 kN, 3.15 kN, 4.15 kN and 5.15 kN). Young's modulus  $E$  of the testing anchor is 31.2GPa calculated by Eq. (3). It is noteworthy that model parameters should be carefully calibrated and determined in the theoretical simulation to mitigate inevitable discreteness between modelling and testing.

Fig. 8 shows the predicted curves compared with the testing pullout creep curves of the anchor head. Correlation coefficients  $R^2$  between the predictions and the model testing data are 0.973, 0.942, 0.964, and 0.923, and the root mean square error (RMSE) are 1.2%, 2.6%, 5.8% and 9.3%, for  $P_0 = 1.75$  kN, 3.15 kN, 4.15 kN and 5.15 kN respectively. The predicted creep curves agree well with the physical model testing data on the whole, which indicates the applicability of the proposed simulation method. However, the prediction accuracy decreases with the pullout load  $P_0$  increasing, especially for the early stage of loading, which may be due to the inherent limitations of Merchant model.

Predictions for the distributions of tensile force and interface shear stress at different times are presented in Figs. 9 and 10, respectively. It can be observed that the distributions of tensile force and interface shear stress are all changed with time for the interface rheological properties between grout and soil. The distribution of tensile force is approximately linear, and the interface shear stress is almost uniform along the anchor, owing to the larger axial stiffness of the anchor than interface shear stiffness. There is something noticeable that the changes of the distributions of both tensile force and interface shear stress are little over time for the same reason. However, the more linear distribution of tensile force and the more uniform distribution of interface shear stress along the anchor are still clearly to be seen. More explicitly, when  $t$  increases from 0 to 50 h, the interface shear stress at the anchor head decreases by 20.9%, 10.3%, 7.7%, and 5.4% for  $P_0 = 1.75$  kN, 3.15 kN, 4.15 kN, and 5.15 kN, respectively; whereas at the anchor toe, the interface shear stress increases by 15.3%, 6.2%, 4.4%, and 2.9%, respectively. This phenomenon indicates the time-dependent mechanical behavior of grouted anchors is also related to the anchor properties and model parameters.

**5. Parametric studies**

The soil properties, bond length and axial stiffness of the anchors can influence the time-dependent behavior of grouted anchors under a coupled mechanism. The impact of soil properties on the grout-soil interface creep behavior can be reflected in the magnitude of Merchant model parameters. Exemplarily, the higher soil viscosity leads to a greater magnitude of the parameter  $\eta$  but a smaller magnitude of the parameter  $G_1$ ; while the higher soil strength corresponds to a greater magnitude of parameter  $G_0$ . Using the presented load transfer model, parametric studies were performed to evaluate the sensitivity of the time-dependent pullout mechanical response on the five model parameters. Table 3 presents parameter magnitude combinations used in

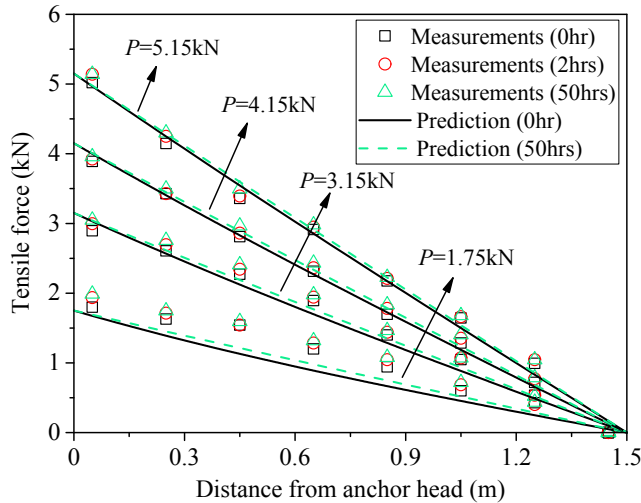


Fig. 9. Predictions for the distributions of tensile force at different time.

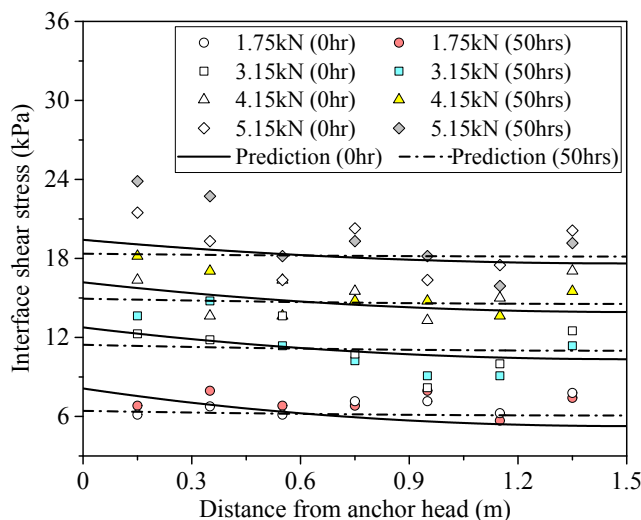


Fig. 10. Predictions for the distributions of interface shear stress at different time.

**4. Theoretical prediction for model test response**

Based on the model test results, theoretical analyses using the above proposed method are conducted for simulating the creep behavior of grouted anchors in laterite. Model parameters have a significant influence on the theoretical prediction results. In this work, Merchant rheological model was adopted for considering the creep interaction between grout and soil. Its three parameters are not only related to material properties, but also stress level (Chen et al., 2016; Sun, 1999). To obtain parameters ( $G_0$ ,  $G_1$ , and  $\eta$ ) of the Merchant rheological model, the least square method is used in the analysis for the pullout creep

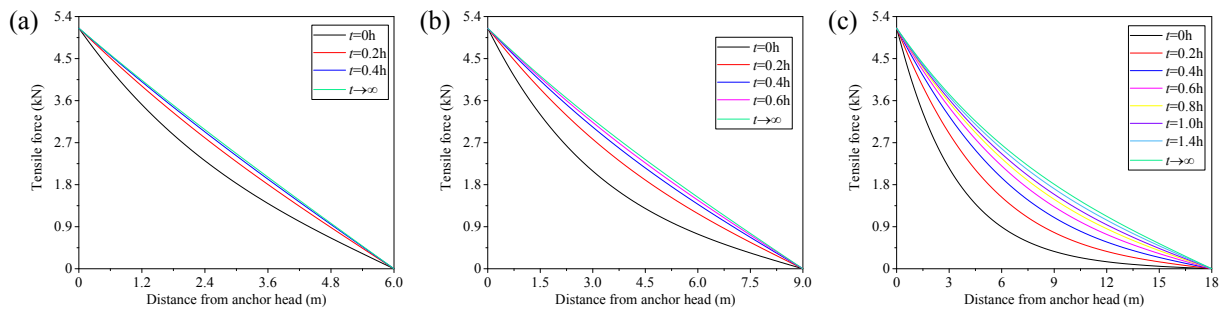


Fig. 11. Time-dependent distributions of tensile force with various bond lengths: (a)  $L = 6$  m; (b)  $L = 9$  m; (c)  $L = 18$  m.

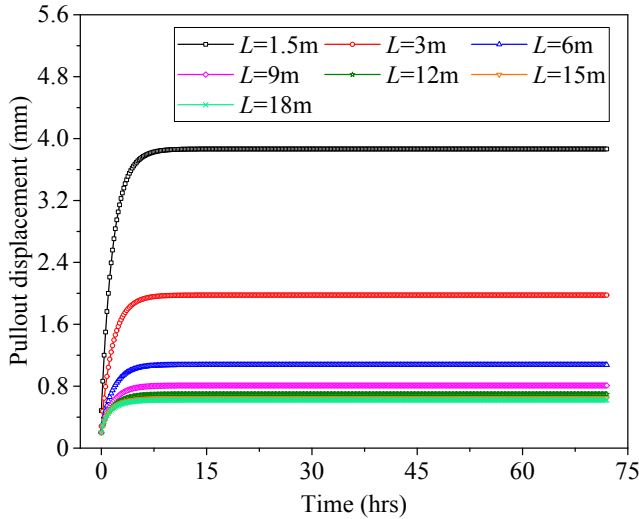


Fig. 12. Pullout creep curves of anchor head with various bond lengths.

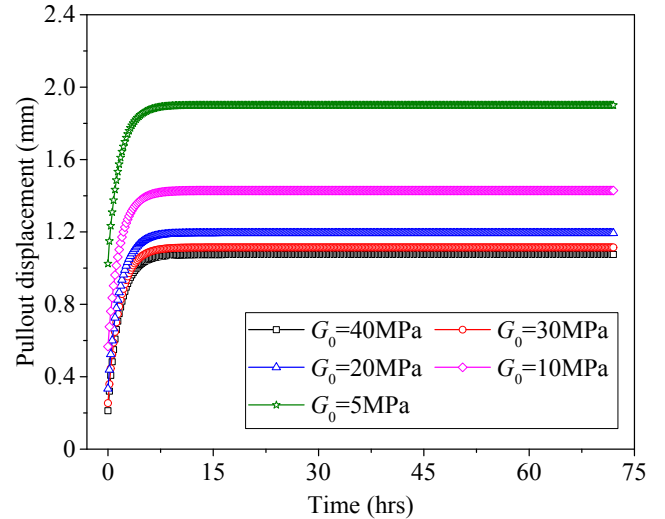


Fig. 14. Pullout creep curves of anchor head with various interface shear modulus  $G_0$ .

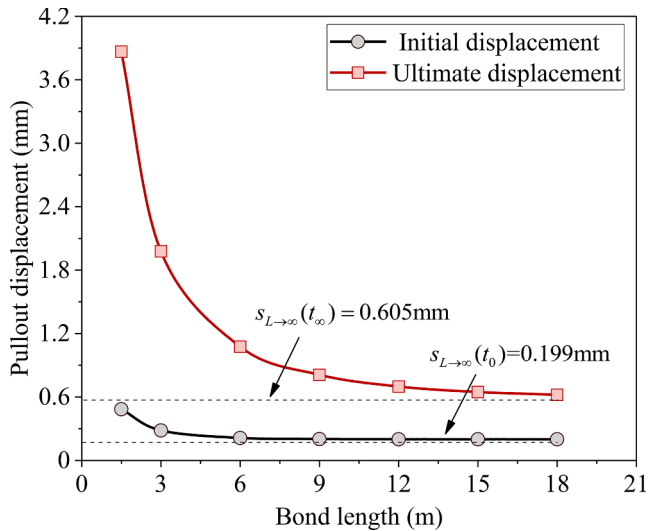


Fig. 13. Pullout displacement versus bond length at the initial and ultimate conditions.

parametric studies. The time interval  $\Delta t$  was set as 0.2 h, and the total time calculated was set as 72 h, which is substantially identical to the loading time of the above model test. The anchor was uniformly divided into 30 units along the axis. Additionally, the pullout load was determined as 5.15 kN.

### 5.1. Effect of bond length $L$ on time-dependent pullout response

The bond length is a key parameter in the design of grouted anchors. Fig. 11 shows the time-dependent distributions of tensile force with various bond lengths. As time increased, the distributions of tensile force tend to be more linear, and the interface shear stresses tend to be more uniform along the anchor. In particular, the change rates of both tensile force and interface shear stress decrease to zero gradually with time increasing. The distributions of both tensile force and interface shear stress at initial moment  $t_0$  and final moment  $t_\infty$  can be calculated by Eqs. (16) and (19), respectively. Additionally, the nonlinearity and time effect of the tensile force distribution become more obvious with bond length  $L$  growing, which indicates that the time-dependent load transfer behavior of grouted anchors is more significantly affected by the interface shear rheological properties between grout and soil.

Fig. 12 shows the pullout creep curves of anchor head with various bond lengths. It can be observed that the pullout displacement increases in decay state with time elapsed, and gradually approaches to a certain value  $s_\infty$ , which can be calculated by Eq. (19). Obviously, for longer bond length  $L$ , the pullout creep displacement tends to be smaller. More specifically, the pullout displacement at the initial and final moments versus bond length is illustrated in Fig. 13. As the bond length increasing, both the initial and ultimate pullout displacement of grouted anchors all decrease, and gradually approach to two certain values named  $s_{L \rightarrow \infty}(x_0, t_0)$  and  $s_{L \rightarrow \infty}(x_0, t_\infty)$ , which can be calculated by Eqs. (29) and (30), respectively. Hence, reducing the long-term displacement of anchorage structure in design practice cannot be achieved by increasing the bond length overly.

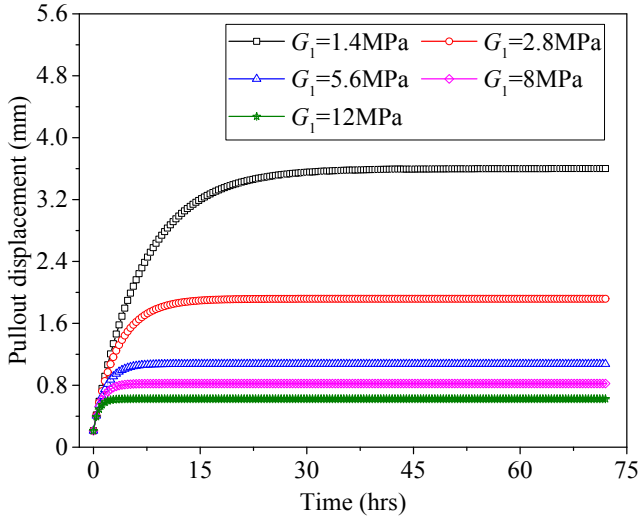


Fig. 15. Pullout creep curves of anchor head with various interface shear modulus  $G_1$ .

$$s_{L \rightarrow \infty}(x_0, t_0) = \lim_{L \rightarrow \infty} \frac{P_0}{(e^{2\beta L} - 1)\beta EA} (1 + e^{2\beta L}) = \frac{P_0}{\beta EA} \quad (29)$$

$$s_{L \rightarrow \infty}(x_0, t_\infty) = \lim_{L \rightarrow \infty} \frac{P_0}{(e^{2\beta^* L} - 1)\beta^* EA} (1 + e^{2\beta^* L}) = \frac{P_0}{\beta^* EA} \quad (30)$$

5.2. Effect of interface shear modulus  $G_0$  on time-dependent pullout response

Fig. 14 shows the pullout creep curves of anchor head with various  $G_0$ . As  $G_0$  increasing, the pullout displacement of grouted anchors decreases, and gradually tends to a certain value named  $s_{G_0 \rightarrow \infty}(x_0, t_\infty)$  (about 0.927 mm in this work) that can be calculated by Eq. (31) when time approaches infinity.

$$s_{G_0 \rightarrow \infty}(x_0, t_\infty) = \lim_{G_0 \rightarrow \infty} \frac{P_0}{(e^{2\beta^* L} - 1)\beta^* EA} (1 + e^{2\beta^* L}) = \frac{P_0}{(e^{2\beta_0 L} - 1)\beta_0 EA} (1 + e^{2\beta_0 L}) \quad (31)$$

where  $\beta_0 = \lim_{G_0 \rightarrow \infty} \beta^* = \sqrt{\frac{G_1 \mu_p}{EA}}$ .

5.3. Effect of interface shear modulus  $G_1$  on time-dependent pullout response

As indicated by Fig 15,  $G_1$  has a great influence on the pullout creep displacement. More specifically, as  $G_1$  increasing, the ultimate pullout displacement of grouted anchors decreases, and gradually tends to a certain value named  $s_{G_1 \rightarrow \infty}(x_0, t_\infty)$  (about 0.212 mm in this work), which

can be calculated by Eq. (32).

$$s_{G_1 \rightarrow \infty}(x_0, t_\infty) = \lim_{G_1 \rightarrow \infty} \frac{P_0}{(e^{2\beta^* L} - 1)\beta^* EA} (1 + e^{2\beta^* L}) = \frac{P_0}{(e^{2\beta L} - 1)\beta EA} (1 + e^{2\beta L}) \quad (32)$$

where  $\beta = \lim_{G_1 \rightarrow \infty} \beta^* = \sqrt{\frac{G_0 \mu_p}{EA}}$ .

5.4. Effect of interface viscosity coefficient  $\eta$  on time-dependent pullout response

Figs. 16 and 17 show the time-dependent distributions of tensile force and pullout creep curves of anchor head with various interface viscosity coefficient  $\eta$ , respectively. It can be observed that the distributions of tensile force and pullout displacement at the initial and final moments are identical with different  $\eta$ , which indicates that  $\eta$  does not influence the initial and ultimate pullout response. But the greater  $\eta$  is, the smaller the variation is in both tensile force and pullout displacement, and the longer the time needs for creep stability. Hence, the creep effect of grouted anchors with greater  $\eta$  would be more obvious.

5.5. Effect of axial stiffness  $EA$  on time-dependent pullout response

Figs. 18 and 19 show the time-dependent distributions of tensile force and pullout creep curves of anchor head with different axial stiffness  $EA$ , respectively. It should be noted that the axial stiffness of the anchor measured in the above model test was 88.2 MN. For greater  $EA$ , the distributions of tensile force for grouted anchors are more linear, and

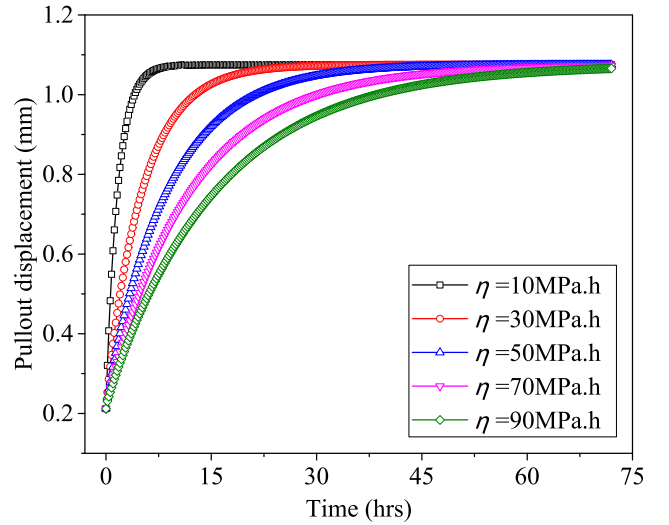


Fig. 17. Pullout creep curves of anchor head with various interface viscosity coefficient  $\eta$ .

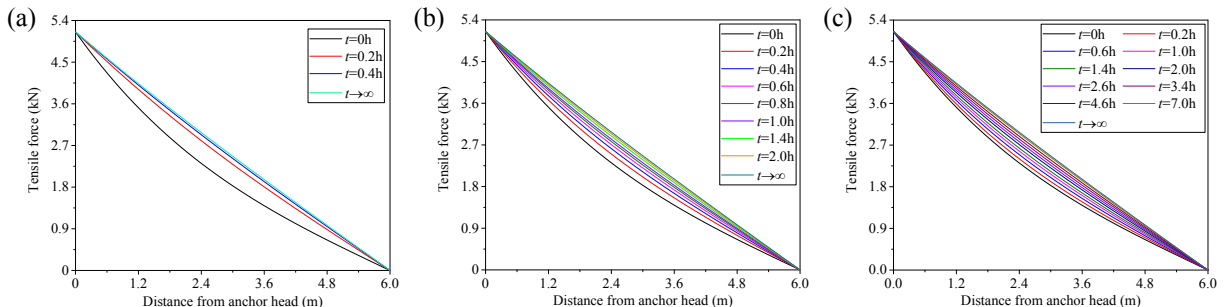


Fig. 16. Time-dependent distributions of tensile force with various interface viscosity coefficient  $\eta$ : (a)  $\eta = 10$  MPa·h; (b)  $\eta = 30$  MPa·h; (c)  $\eta = 90$  MPa·h.

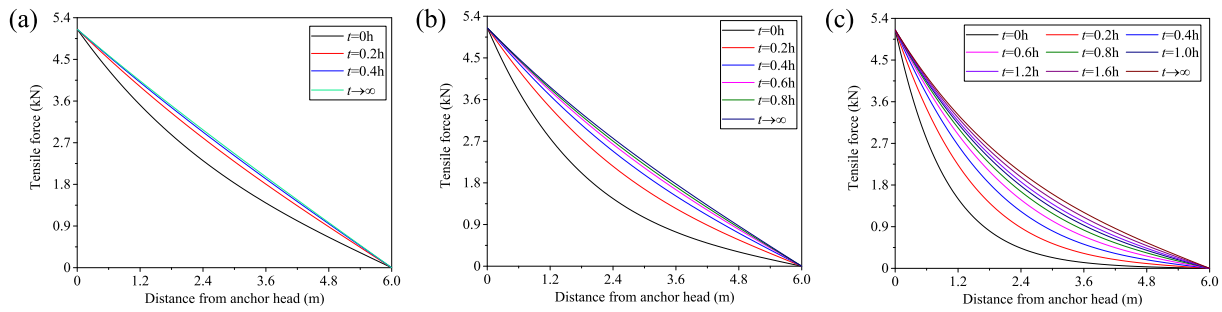


Fig. 18. Time-dependent distributions of tensile force with various axial stiffness EA: (a) EA = 88.2 MN; (b) EA = 28.3 MN; (c) EA = 7.1 MN.

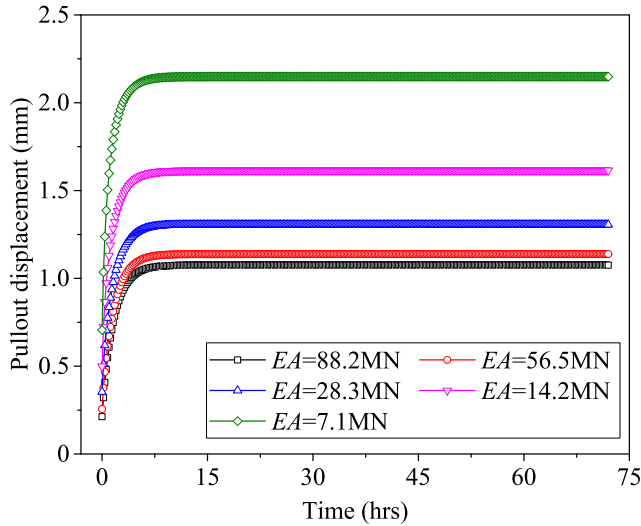


Fig. 19. Pullout creep curves of anchor head with various axial stiffness EA.

the shear stresses are more uniform along the anchor, but the creep effect tends to be weakened. Additionally, with the axial stiffness increasing, the creep pullout displacement decreases, and the pullout displacement at the initial and final moments all tend to certain values that can be calculated by Eqs. (34) and (35), which are 0.114 mm and 0.927 mm in this work, respectively. This demonstrates that goal of the pullout displacement reduction cannot be achieved by increasing the axial stiffness excessively in anchorage structures. Hence, avoiding the excessive amount of stiffness value in grouted anchors is encouraged in design practice.

$$s_{EA \rightarrow \infty}(x_0, t_0) = \lim_{EA \rightarrow \infty} \frac{P_0}{(e^{2\beta L} - 1)\beta EA} (1 + e^{2\beta L}) = \frac{P_0}{\mu_p L G_0} \quad (34)$$

$$s_{EA \rightarrow \infty}(x_0, t_\infty) = \lim_{EA \rightarrow \infty} \frac{P_0}{(e^{2\beta^* L} - 1)\beta^* EA} (1 + e^{2\beta^* L}) = \frac{(G_0 + G_1)P_0}{G_0 G_1 \mu_p L} \quad (35)$$

## 6. Conclusions

Creep pullout model test for full-length-bond grouted anchors embedded in laterite was carried out using a specially designed pullout setup. Time-dependent pullout response, i.e. tensile force and shear stress distributions over bond length, and pullout displacement creep curves of anchor head were measured in the physical model test. The time-dependent load transfer analysis method on the grouted anchor embedded in laterite was developed by modelling the anchor-laterite interface shear creep behavior using Merchant rheological model.

By comparing measurements obtained in model test and predictions derived from load transfer simulation for pullout creep response, the

effectiveness and applicability of the presented analysis method were essentially examined and verified. Based on the analysis method, the impacts of bond length, axial stiffness of the anchor, and interface creep model parameters on the time-dependent pullout response of grouted anchors were further investigated parametrically. The main conclusions can be summarized as follows:

- The specially designed creep pullout setup and test protocol presented in this work are capable of measuring the time-dependent pullout response of grouted anchors embedded in laterite with the soil conditions and anchor dimensions well controlled.
- The creep pullout displacement of grouted anchors embedded in laterite was mainly constituted by the grout - soil interface shear displacement rather than the tensile deformation of anchor owing to the comparatively prevailing anchor axial stiffness than the interface shear stiffness.
- Both test measurements and load transfer modelling predictions reveal that the linearity of tensile force distribution and the uniformity of interface shear stress distribution over bond length, enhanced over the elapsed loading time.
- Shear modulus relevant parameters in Merchant rheological modelling of interface creep behavior affect remarkably the pullout creep displacement.
- The increasing viscosity coefficient in Merchant rheological modelling of interface creep behavior corresponds to more obviously observed pullout creep behavior, but does not change pullout response at initial and ultimate conditions.
- Excessively increasing bond length and axial stiffness is not capable of reducing the ultimate pullout displacement for grouted anchors in laterite, and is not recommended in design practice.

Overall, the grout - soil interface creep behavior of grouted anchors embedded in laterite was investigated thoroughly by incorporating creep pullout model testing and load transfer modelling in this work. The presented creep pullout testing protocol and rheological modelling technique can provide insights into understandings of time-dependent behavior, and facilitate the service life design practice for grouted anchors embedded in laterite. It is noted that further investigations on coupled interactions among interface creep, soil creep and anchor creep are undergoing by the authors, which is indeed a more accurate modelling of time-dependent behavior of grouted anchors.

## CRedit authorship contribution statement

**Changfu Chen:** Supervision, Methodology, Funding acquisition. **Shimin Zhu:** Investigation, Data curation, Writing - original draft, Writing - review & editing. **Genbao Zhang:** Writing - review & editing. **Fengshan Mao:** Investigation, Writing - original draft. **Huan Cai:** Writing - original draft.

## Declaration of Competing Interest

The authors declare that they have no known competing financial interests or personal relationships that could have appeared to influence the work reported in this paper.

## Acknowledgments

This research was sponsored by the National Natural Science Foundation of China (grant numbers 41572298, 51978254, 51908201). The authors appreciate their financial support.

## References

- Borana, L., Yin, J.H., Singh, D.N., Shukla, S.K., Pei, H.F., 2017. Influences of initial water content and roughness on skin friction of piles using FBG technique. *Int. J. Geomech.* 17 (4), 04016097. [https://doi.org/10.1061/\(ASCE\)GM.1943-5622.0000794](https://doi.org/10.1061/(ASCE)GM.1943-5622.0000794).
- Chen, G.Q., Chen, T., Chen, Y., Huang, R.Q., Liu, M., 2018. A new method of predicting the prestress variations in anchored cables with excavation unloading destruction. *Eng. Geol.* 241, 109–120. <https://doi.org/10.1016/j.enggeo.2018.05.015>.
- Chen, J., Dai, F.C., Xu, L., Chen, S., Wang, P.F., Long, W., Shen, N.Q., 2014. Properties and microstructure of a natural slip zone in loose deposits of red beds, southwestern China. *Eng. Geol.* 183, 53–64. <https://doi.org/10.1016/j.enggeo.2014.10.004>.
- Chen, C.F., Liang, G.T., Tang, Y., Xu, Y.L., 2015. Anchoring solid-soil interface behavior using a novel laboratory testing technique. *Chin. J. Geotech. Eng.* 37 (6), 1115–1122. <https://doi.org/10.11779/CJGE201506018>.
- Chen, C.F., Liu, J.B., Xu, Y.L., Zhang, G.B., 2016. Tests on shearing creep of anchor-soil interface and its empirical model. *Chin. J. Geotech. Eng.* 38 (10), 1762–1768. <https://doi.org/10.11779/CJGE201610003>.
- Chen, C.F., Zhu, S.M., Gao, J., Wen, Y.K., Mao, F.S., 2019. Kriging method-based creep model for anchor-soil interface considering grouting pressure. *Chin. J. Geotech. Eng.* 41 (S1), 125–128. <https://doi.org/10.11779/CJGE2019S1032>.
- Chen, C.F., Liu, S.M., Mao, F.S., Zhang, G.B., 2019. Characterization and modelling of coupled consolidation-creep behavior of red clay. *J. Eng. Geol.* 27 (04), 723–728. <https://doi.org/10.13544/j.cnki.jeg.2018-330>.
- Chen, C.F., Zhang, G.B., Zornberg, J.G., Zheng, X.X., 2019. Element nail pullout tests for prediction of soil nail pullout resistance in expansive clays. *Geotech. Test. J.* 42 (5), 1274–1297. <https://doi.org/10.1520/GTJ20170431>.
- Cheng, Q., Kong, X.B., Huang, S.B., Zhou, Y.J., 2004. The distributes and geologic environment characteristics of red beds in china. *J. Eng. Geol.* 12 (1), 34–40.
- Chu, L.M., Yin, J.H., 2005. Comparison of interface shear strength of soil nails measured by both direct shear box tests and pullout tests. *J. Geotech. Geoenviron. Eng.* 131, 1097–1107. [https://doi.org/10.1061/\(ASCE\)1090-0241\(2005\)131:9\(1097\)](https://doi.org/10.1061/(ASCE)1090-0241(2005)131:9(1097)).
- Cooke, R.W., Price, G., Tarr, K., 1979. Jacked piles in London Clay: a study of load transfer and settlement under working conditions. *Géotechnique* 29 (2), 113–147. <https://doi.org/10.1680/geot.1979.29.2.113>.
- Ehrlich, M., Silva, R.C., 2015. Behavior of a 31 m high excavation supported by anchoring and nailing in residual soil of gneiss. *Eng. Geol.* 191, 48–60. <https://doi.org/10.1016/j.enggeo.2015.01.028>.
- EI Menoufy, A., Soudki, K., 2014. Effects of various environmental exposures and sustained load levels on the service life of postinstalled adhesive anchors. *J. Mater. Civ. Eng.* 26 (5), 863–871. [https://doi.org/10.1061/\(ASCE\)MT.1943-5533.0000878](https://doi.org/10.1061/(ASCE)MT.1943-5533.0000878).
- Farmer, I.W., 1975. Stress distribution along a resin grouted rock anchor. *Int. J. Rock Mech. Min. Sci. Geomech. Abstr.* 12, 347–351. [https://doi.org/10.1016/0148-9062\(75\)90168-0](https://doi.org/10.1016/0148-9062(75)90168-0).
- Gurpersaud, N., Vanapalli, S.K., Sivathayalan, S., 2013. Semiempirical method for estimation of pullout capacity of grouted soil nails in saturated and unsaturated soil environments. *J. Geotech. Geoenviron. Eng.* 139 (11), 1934–1943. [https://doi.org/10.1061/\(ASCE\)GT.1943-5606.0000883](https://doi.org/10.1061/(ASCE)GT.1943-5606.0000883).
- Hong, C.Y., Zhang, Y.F., Zhang, Y.W., Borana, L., Wang, R.F., 2017. New LGFBG-based structural integrity evaluation method for cement-grouted soil nails. *Int. J. Geomech.* 17 (8), 04017026. [https://doi.org/10.1061/\(ASCE\)GM.1943-5622.0000910](https://doi.org/10.1061/(ASCE)GM.1943-5622.0000910).
- Hong, C.Y., Liu, Z.X., Zhang, Y.F., Zhang, M.X., Borana, L., 2017. Influence of critical parameters on the peak pullout resistance of soil nails under different testing conditions. *Int. J. Geosynth. Ground Eng.* 3, 19. <https://doi.org/10.1007/s40891-017-0095-5>.
- Huang, Y., Fu, B.C., 1998. Research on laterization and specific property of laterite in engineering geology. *Chin. J. Geotech. Eng.* 20 (3), 40–44.
- Huang, M.H., Zhou, Z., Yue, S., He, J.P., Ou, J.P., 2012. A novel durable intelligent fiber reinforced polymer anchor with embedded optical fiber Bragg grating sensors. *Sci. China: Technol. Sci.* 55 (5), 307–314. <https://doi.org/10.1007/s11431-012-4761-5>.
- Kim, Y., Lee, S., Jeong, S., Kim, J., 2013. The effect of pressure-grouted soil nails on the stability of weathered soil slopes. *Comput. Geotech.* 49, 253–263. <https://doi.org/10.1016/j.compgeo.2012.12.003>.
- Kränkell, T., Lowke, D., Gehlen, C., 2015. Prediction of the creep behaviour of bonded anchors until failure—A rheological approach. *Constr. Build. Mater.* 75, 458–464. <https://doi.org/10.1016/j.conbuildmat.2014.11.048>.
- Lin, Z.Y., 1989. Discuss the engineering classification of the red clay. *Chin. J. Geotech. Eng.* 11 (1), 87–98.
- Luo, Y.H., Zhu, C.L., Li, J.D., 2003. Research for distortion-destruction mechanism of slopes of red strata in Yunnan province and their hazard control. *Rock. Soil Mech.* 24 (5), 836–839. <https://doi.org/10.16285/j.rsm.2003.05.037>.
- Ma, S.Q., Zhao, Z.Y., Nie, W., Gui, Y.L., 2016. A numerical model of fully grouted anchors considering the tri-linear shear bond-slip model. *Tunn. Undergr. Space Technol.* 54, 73–80. <https://doi.org/10.1016/j.tust.2016.01.033>.
- Martín, L.B., Tijani, M., Hadj-Hassen, F., 2011. A new analytical solution to the mechanical behaviour of fully grouted rockanchors subjected to pull-out tests. *Constr. Build. Mater.* 25 (2), 749–755. <https://doi.org/10.1016/j.conbuildmat.2010.07.011>.
- Ren, F.F., Yang, Z.J., Chen, J.F., Chen, W.W., 2010. An analytical analysis of the full-range behaviour of grouted rockanchors based on a tri-linear bond-slip model. *Constr. Build. Mater.* 24, 361–370. <https://doi.org/10.1016/j.conbuildmat.2009.08.021>.
- Shi, K.Y., Wu, X.P., Liu, Z., Dai, S.L., 2019. Coupled calculation model for anchoring force loss in a slope reinforced by a frame beam and anchor cables. *Eng. Geol.* 260, 105245. <https://doi.org/10.1016/j.enggeo.2019.105245>.
- Su, L.J., Yin, J.H., Zhou, W.H., 2010. Influences of overburden pressure and soil dilation on soil nail pull-out resistance. *Comput. Geotech.* 37 (4), 555–564. <https://doi.org/10.1016/j.compgeo.2010.03.004>.
- Sun, J., 1999. *Rheological Behavior of Geomaterials and its Engineering Applications*. China Architecture and Building Press, Beijing, pp. 60–61.
- Tan, T.K., Kang, W.F., 1980. Locked in stresses, creep and dilatancy of rocks, and constitutive equations. *Rock Mech.* 13 (1), 5–22. <https://doi.org/10.1007/BF01257895>.
- Tan, L.R., Kong, L.W., 2006. *Soil Geotechnolgy in Special Geotechnical and Engineering*. Science Press, Beijing, pp. 201–248.
- Wu, G.J., 2009. *Time-dependent Behaviour of Rock Mass and ITS Reliability on Anchoring in Underground Engineering*. Institute of Rock and Soil Mechanics Chinese Academy of Sciences, Wuhan, pp. 18–41.
- Xu, H.F., Lu, H.B., Qin, Q.H., 2002. Creep damage effects of pulling grouting anchor in soil. *Chin. J. Geotech. Eng.* 24 (1), 61–63.
- Yang, M.J., Zhao, Y.M., Zhang, N., 2014. Creep behavior of epoxy-bonded anchor system. *Int. J. Rock Mech. Min. Sci.* 67, 96–103. <https://doi.org/10.1016/j.ijrmm.2014.02.001>.
- Ye, X.Y., Wang, S.Y., Wang, Q., Sloan, S.W., Sheng, D.C., 2017. Numerical and experimental studies of the mechanical behaviour for compaction grouted soil nails in sandy soil. *Comput. Geotech.* 90, 202–214. <https://doi.org/10.1016/j.compgeo.2017.06.011>.
- Zhang, G.B., Chen, C.F., Zornberg, J.G., Morsy, A.M., Mao, F.S., 2020. Interface creep behavior of grouted anchors in clayey soils: effect of soil moisture condition. *Acta Geotech.* 15, 2159–2177. <https://doi.org/10.1007/s11440-019-00907-6>.
- Zhang, Z.L., Wang, T., Wu, S.R., Tang, H.M., Liang, C.Y., 2018. Dynamics characteristic of red clay in a deep-seated landslide, Northwest China: An experiment study. *Eng. Geol.* 239, 254–268. <https://doi.org/10.1016/j.enggeo.2018.04.005>.
- Zhang, M., Yin, Y.P., Huang, B.L., 2015. Mechanisms of rainfall-induced landslides in gently inclined red beds in the eastern Sichuan Basin, SW China. *Landslides* 12 (5), 973–983. <https://doi.org/10.1007/s10346-015-0611-4>.
- Zhang, C.C., Zhu, H.H., Xu, Q., Shi, B., Mei, G.X., 2015. Time-dependent pullout behavior of glass fiber reinforced polymer (GFRP) soil nail in sand. *Can. Geotech. J.* 52, 671–681. <https://doi.org/10.1139/cgj-2013-0381>.
- Zhu, S.M., Chen, C.F., Gao, J., 2019. Creep model of red clay based on ANFIS neural network. *J. Hunan Univ. Nat. Sci.* 46 (11), 137–145. <https://doi.org/10.16339/j.cnki.hdxzbk.2019.11.016>.
- Zhu, H.H., Yin, J.H., Yeung, A.T., Jin, W., 2011. Field pullout testing and performance evaluation of GFRP soil nails. *J. Geotech. Geoenviron. Eng.* 137 (7), 633–642. [https://doi.org/10.1061/\(ASCE\)GT.1943-5606.0000457](https://doi.org/10.1061/(ASCE)GT.1943-5606.0000457).